Skoltech

Proceedings of the Skoltech Energy PhD Seminar

2020/21

Skolkovo Institute of Science and Technology Skolkovo
Innovation Center, Building 3
www.skoltech.ru/en

Proceedings of the Skoltech Energy PhD Seminar 2020/21

The *Proceedings* are a collection of the original research papers written by the participants of the fifth Skoltech Energy PhD Seminar in the 2020-2021 academic year.

The Skoltech PhD Energy Seminar unites the students enrolled to Skoltech PhD Programs in *Materials Science & Engineering*, *Physics*, *Engineering Systems*, and *Petroleum Engineering*, associated with the Centers of Energy Science and Technology, Photonics and Quantum Materials, Hydrocarbon Recovery, and some others.

The Seminar promotes the exchange of knowledge, methodologies, and research challenges across the fundamentally different scientific areas aligned with the Skoltech vision of multidisciplinary research and education oriented to innovation. To this aim, the Seminar maintains a broad scientific scope, that is, a whole diversity of the research topics to which "Energy" and "Materials" keywords are applicable. This year the Seminar collected a few contributions mostly lying within the "Materials" mainstream.

The Seminar engages the PhD students in professional academic communication activities based on the principles of ethics and peer review. During the Seminar, students are required to present the results of their research, write a contribution for the Proceedings according to a template, and peer review two papers submitted by the Seminar participants.

In preparation for the *Proceedings*, each paper was anonymously reviewed by two peers and checked by a language instructor. The final versions had to incorporate comments from the referees and editors to be accepted for the *Proceedings*.

We believe that this exercise provides the students with a useful experience as well as a publishing opportunity in the *Proceedings*. We appreciate that the students may prefer to disseminate their outstanding research results in more impactful publications.

We are pleased to use this occasion to congratulate the participants of the past Skoltech PhD Energy Seminars who have received Skoltech PhD degree this academic year, Mikhail Pugach and Andrey Churkin (*Engineering systems*), Andrei Tarkhov (*Physics*), Aysylu Askarova, Anastasia Ivanova, Lyudmila Khakimova, and Aliya Mukhametdinova (*Petroleum Engineering*).

We appreciate the concerted efforts and devotion of all the Seminar attendees and the contributions of their supervisors. We are grateful to the Skoltech Deans of Education Dr. Anna Derevnina and Prof. Clement Fortin for supporting the Seminar initiative and to Dr. Anna Sharova (Institute for African Studies, RAS), Ksenia Rogova and Ekaterina Guseva for helping with the Seminar and publication of the *Proceedings*.

Alexei Buchachenko (Seminar instructor)
Elizaveta Tikhomirova

June 2021

CONTENTS

Research articles

On the Recent Developments in Electrospinning to Produce Hierarchically Organized Composites for Separator Membranes

Y. Kan*, Alexey I. Salimon, Alexander M. Korsunsky

Abstract

This research article aims to reveal the potential of electrospinning for separator applications. The product of electrospinning is a nano- or microfiber that could serve as a building unit for multilayered structures with high permeability, which, in turn, could be used as a filter or battery separators. The abundance of polymers supporting electrospinning opens up the opportunity toward building a composite. A series of composite modifying inorganic nanoparticles allows improving of the mechanical and thermal stability of separator. In this work, we describe the fabrication of fibers build with the set-up produced in FabLab and Machine Shop Shared Facility at Skoltech. Recent studies showed the involvement of electrospinning in battery separators field. The preliminary results of electrospun material reported cover the morphology characterization for the obtained fibrous membranes yield from the composition of polyvinyl alcohol solution with additive nanoparticles of SiO_2.

Index Terms

Electrospinning, fibers, composite, polyvinyl alcohol, separators.

* Yuliya Kan is doctoral student with the Center for Energy Science and Technology, Skolkovo Institute of Science and Technology, Skolkovo Innovation Center, Building 3, Moscow 121205, Russia (e-mail: Yuliya.Kan@skoltech.ru).

Alexey I. Salimon is Senior Research Engineer at the Hierarchically Structured Materials (HSM) lab, Center for Energy Science and Technology, Skolkovo Institute of Science and Technology, Skolkovo Innovation Center, Building 3, Moscow 121205, Russia (e-mail: A.Salimon@skoltech.ru).

Alexander M. Korsunsky is Head of the Multi-Beam Laboratory for Engineering Microscopy (MBLEM), Professor of Engineering Science, Department of Engineering Science, University of Oxford, Parks Road, Oxford OX1 3PJ, UK and Professor of Center for Energy Science and Technology, Skolkovo Institute of Science and Technology, Skolkovo Innovation Center, Building 3, Moscow 121205, Russia (e-mails: alexander.korsunsky@eng.ox.ac.uk, a.korsunsky@skoltech.ru)

I. NOMENCLATURE

DMA	Dimethylacetamide
PAN	Polyacrylonitrile
PP	Polypropylene
PET	Polyethylene terephthalate
PVA	Polyvinyl alcohol
PVDF	Polyvinylidene fluoride

II. INTRODUCTION

THERE is a growing demand for the energy supply with the spread of portable devices as smartphones, laptops, home devices and electric cars. Due to the high energy density of Li-ion batteries, their consumption was increased worldwide. The Li-ion batteries have four main components: cathode, anode, electrolyte and separator. The transfer of Li ions provides the charging and discharging electrochemical processes on the surfaces of electrodes. Current research is aimed at improving the battery charge-discharge parameters to extend the life cycle and avoid the formation of defects such as dendrite structures caused by the rapid migration of Li ions. The optimal thermal range is 60-70˚C for the life cycle of Li-ion batteries that limits the usage of Li-ion batteries in the higher thermal range and working constructions [1]. Therefore, the development of separator should meet the strategy to increase of the operational thermal range for Li-ion batteries. In case the battery is exposed to external conditions like high temperatures, the polyolefin separators start melting at 130˚C and degradation which often leads to internal short circuits and subsequent thermal runaway (TR) and potential explosion [2]. The functions of separator include the support of the battery life cycle preventing the short circuit, and simultaneously provide Li ionic transport between electrodes.

Therefore, the separator should consists of a membrane with dielectric properties with the thermal resistance to retain its morphology and interconnected porosity for ion migration. Thus, the structure of separator should provide long-term thermal and chemical stability in the electrolyte during the charge-discharge processes. In case of the fast charging the Li ions with intensive rate, the lithium ions form dendrites on the surface of electrodes that causes the battery damage.

The market of commercial separators contains the following segments: microporous membranes, ceramics, nonwoven mats, and composite membranes. The microporous membranes segment has occupied a significant share of the global battery separator materials market in the last decades. These separators possess low acid solubility, good oxidation resistance, good wettability, low electrical resistance, and high porosity [3].

Commercially used microporous membranes (Celgard) are composed of polyolefins: polypropylene (PP) and polyethylene (PE) based structures. Celgard 2325 consists of a three-layer of PP/PE/PP; Celgard 2500 consists of a monolayer membrane of PP obtained by crazing method via deformation below the melting point. According to the manufacturer's information, the porosity reaches 39% for Celgard 2325 and 55% for Celgard 2500, respectively [4]. The thickness of the membrane is 25 μm for both products. Pores near 24 nm and 64 nm supported the required ion migration for Celgard 2325 and Celgard 2500, respectively. The PE layer has a low melting point of 135˚C that can act as a thermal fuse and block ions direction when it is close to its melting temperature. Simultaneously, the PP layer preserves the dimensional structure and mechanical strength of a composite using a higher melting property of 165˚C. Using the synergy input of two materials, the three-layered composite prevents the short-circuiting [5]. The recent studies of separators aimed at the increase of wetting with ester carbonate electrolytes and thermal stability of separator structure to extend the safety of using Li-ion batteries [2]. The widely used polyolefin separators stop retaining the porous structure of PE layer at temperatures above 130°C that leads to the loss of the dimensional stability and functionality [6]. One of the recent improvements of conventional separators is aimed to increase a thermal dimensional resistance of separators [7], [8].

The electrospinning captured the attention as a simple and adaptable technology to fabricate polymeric composites [9]. There is a study where the PP separator was modified with the help of electrospun PET coating [10]. The study of composite separator PP/PET showed that after the heating range at 120-180 ˚C the thermal shrinkage was less than the commercial PP separator demonstrated. The electrospun PET coating increased the thermal stability of PP/PET composite where the PET retained the wholeness of separator up to 248˚C after the PP separator could thermally shutdown at 169˚C. The hierarchical composite PP/PET was mounted in the cell with the $LiFePO_4$ cathode to compare the discharge capacity of the cell with the commercial PP microporous separator. The cycle performance of cells with the electrospun based composite PP/PET showed a higher discharge capacity of 149 mAh/g after 50 cycles than 134 mAh/g for cell with PP separator. The ionic conductivity of PP/PET composite measured at room temperature was higher at 0.782 mS/cm in comparison to the PP separator with 0.503 mS/cm. Hence, electrospinning is expected to be a robust tool to build up a separator membrane with the optimal Li ionic transfer for practical applications.

The technology of electrospinning includes the fabrication of the polymer fibers lengthened by the electric field generated by the high voltage power supply. When the applied electric field forces overcome the surface tension, the elongated drop of polymer facilitates the fiber during the evaporation of the solvent. The collected fibers form the network structure with a high surface-to-volume ratio and porosity, which facilitate the transfer of lithium ions. This method can produce nonwoven hierarchical organized structures from diverse polymer mesh. Such polymers as PVDF [11], PET [10], PAN [12], PVA [12], [13] are used to design fibrous materials by the electrospinning for separator fabrication.

The host polymer solution could be based on PVDF as one of the polymers with a high thermal stability [14]-[18]. PVDF solution with a mixture of solvents (acetone/DMA = 7/3 by weight) facilitated electrospinning with average fiber diameter of 0.45 μm and mean pore size 1.1 μm that retained 80% of the initial absorbed volume of electrolyte [11]. However, the low mechanical properties and hydrophobicity of PVDF hinder the spread of polymer. Nanoparticles of Al_2O_3 were added into the polymer solution to mitigate these disadvantages and improve wettability [18]. Despite these facts, the hazardous solvents of PVDF prevent the membrane fabrication and stimulate the study and design of other, safer and more human friendly compositions.

PAN is one of the potential components for the separators due to the excellent thermal stability and high electrolyte uptake. The composite PAN/PVA/MA performed the reduced contact angle 42˚ in comparison with 85˚ for pure PAN that evidenced the increased wettability of this PAN/PVA/MA composite [12]. This polymer allows the fabrication of separators with increased wettability.

The polymers like polyvinyl alcohol (PVA) could be dissolved with a safe solvent as distilled water under heating up to 90˚C to form a homogeneous solution. To improve the mechanical stability, the PVA is mixed with a crosslinking component such as malonic acid (MA). The PVA based solution supports the repetitive electrospinning process. Polyvinyl alcohol serves as a binder for polymer meshes and is well-known as a ‘green’ and safe polymer. Due to these properties, the PVA based compositions are easy to handle to prepare the electrospun solutions up to 10-16 wt.% [13], [19], [20]. Moreover, the high dielectric strength, good charge storage capacity and dopant dependent electrical properties could be useful for membrane fabrication. Besides, the studies reported the impact of PVA on the surface wettability of separator [12]. However, the low mechanical properties of PVA fibers are not sufficient for the separator membrane and still under study to be modified. Hence, there are some modifying components (lignin, ceramic nanoparticles) embedded in the polymer composition.

Lignin is a biopolymer derived from plants, considered as a component that produces an environmentally friendly, inexpensive, nonwoven separator membrane. The lignin/PVA membrane has superior wettability and electrolyte uptake over the Celgard separator, while the mechanical properties of separator are still the subject of improvement [21].

However, the overall drawbacks such as the mechanical strength and thermal stability of the obtained membranes prevent the spread of electrospinning and need to be optimized. The researchers try to fix the polymer meshes using the inorganic particles (SiO_2, Al_2O_3, ZrO_2) [22].

The research of electrospun PVA/SiO_2 nanofiber separator membrane demonstrated the greater electrochemical values of electrolyte uptake and ionic conductivity in comparison with the microporous PP membrane [13]. The incorporation of silica caused an improvement of electrochemical properties due to the affinity of particles to the liquid electrolyte and their high porosity. The higher mass fraction of silica caused the decrease of average fiber diameter and presented the defects like beads on fibers. However, the current issue is an agglomeration of particles that leads to the low electrospinning of solutions. It indicates the modern problem of using silica in the electrospun membranes. The authors of that article tried to solve that issue by means of a sol-gel process that allowed homogeneous distribution of the synthesized silica [13].

Nanosilica (SiO_2) is one of the most widely used nanomaterials due to its thermal resistance, lyophilicity and chemical inertness. Moreover, it has a higher dielectric ratio and lower dielectric loss than other inorganic fillers. The preparation of a modified PP separator with the nonwoven coating of SiO_2/PVA layer showed the prospects for lithium batteries [9].

Spraying of inorganic nanoparticles ZrO_2 at the top of PVA fibers was investigated to study the multilayered PVA-electrospun composite for electrochemical applications. PVA/ZrO_2 multilayered composite showed thermal resistance at 160°C, ionic conductivity of 2.19 mS/cm, and satisfactory electrolyte wettability and tensile strength [20].

There are two issues to handle the nanoparticle for the separator applications. One of these is the problem of homogeneous distribution in the membrane without the formation of aggregates [22]. Moreover, the inorganic nanoparticles increase the mechanical stability and may cause the difficulty to mount the separator into the cell due to its brittleness and fragile [22]. It is a limiting factor of using the nanoparticles in the field of battery separator. The recent studies are aimed to solve this problem and distribute the nanoparticles throughout the composite and provide tensile fibrous structure [13], [20].

In our paper, the modification of fibers with nanoparticles is considered as a solution for the separators of Li-ion batteries. The involvement of electrospinning makes it possible to fabricate the nanofibrous multilayered composite with nanoparticles. An optimal composition of components is under the scope of a research project.

III. MATERIALS AND METHODS

A. Materials

Polyvinyl alcohol powder was supplied from RusChem, Moscow, Russia. Colloidal silica suspension OP-S Non-Dry was obtained from Struers, USA. Copper TEM grids were supplied from the Agar Scientific Ltd, UK.

B. Electrospinning process

Polyvinyl alcohol powder was dissolved in the distilled water at 80°C for 3 hours in a magnetic stirrer. The host polymeric solution had a solid content of 10 wt.% in the solvent where the concentration was given from the references [13], [19], [20]. The 10 wt.% solution of PVA was cooled down and mixed with the colloidal suspension of SiO_2 nanoparticles OP-S Non-Dry in a ratio of PVA solution to the solution of silica (90:10) and (85:15). Then, the PVA/OP-S solutions were homogenized for 3 hours at room temperature in the magnetic stirrer. The polymeric solutions were placed in a 20 ml syringe with a needle of 21G in the laboratory apparatus consisting of a syringe pump, a 22 kV high-voltage direct-current power supply (Fig. 1). The flow rate of the pump was 1 ml/h, and the tip-to-collector distance was set at 15 cm. The electrospinning set up has two types of fiber collectors: rotating mandrel and the holder for the flat aluminum target.

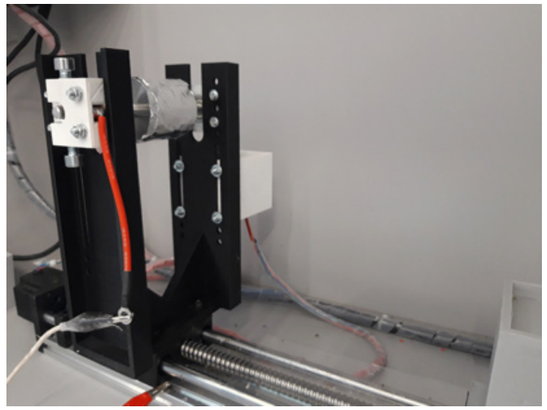

Fig. 1. The representation of electrospinning equipment constructed by Fablab

The rotating mandrel was placed at the tunable distance in front of the syringe pump. The electric field was applied to the connected electrodes between the syringe needle and mandrel. The polymeric solution was loaded in the syringe and was ejected at the defined flow rate by the syringe pump. The rotation speed and the change of distance could be adjusted.

The fibers of 85PVA15OP-S were collected on the carbon lacey copper TEM grids during 1 min of electrospinning at 18 kV. The TEM grid was mounted at the flat target to obtain a monolayer of fibrous coating for TEM characterization. After the sputtering, the samples were dried at room temperature before the measurements.

C. Morphology characterization of obtained fibers

1) Scanning electron microscopy (SEM)

The morphology of the nanofiber separator was characterized using scanning electron microscope VEGA 3 (Tescan, Brno, Czech Republic) with the accelerating voltage of 6 kV and 12 kV and analyzed with Tescan software. SEM images with high resolution were obtained from FEI Helios G4 Plasma FIB Uxe with voltage 2 kV and 3 kV.

2) Transmission electron microscopy (TEM)

The morphology of the silica nanospheres dispersed in the fibrious mat was observed using TEM) on FEI Titan Themis Z instrument operating with an acceleration voltage of 120 kV.

IV. RESULTS AND DISCUSSIONS

Diameter of the nanofibers 90PVA10OP-S ranges from 80 to 110 nm in Fig. 2. Thus, the SEM images prove the formation of PVA/OP-S nanofibers. There is no bead formation but some clusters of particles are observed. It should be mentioned that the beads are considered as the defect of electrospinning that could be caused by such factors as low polymer concentration and solution viscosity that does not support stable fiber formation [23]. The fabricated polymer solutions were electrospun into the fibers that contain some clusters which morphology differs with beads. Both compositions have the agglomerates of nanoparticles that seemed to be immersed in the depth of fiber.

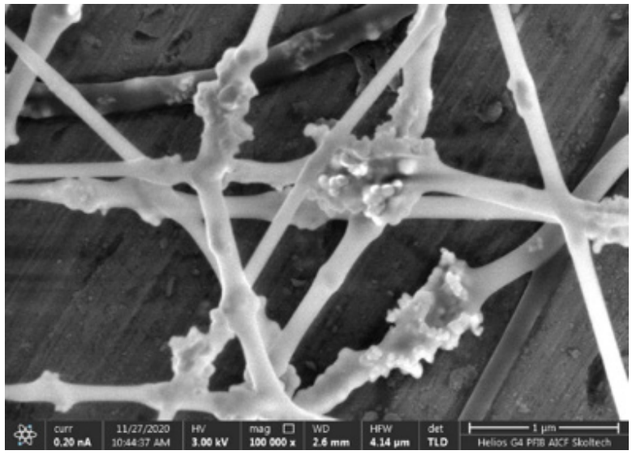

Fig. 2. SEM imaging of morphology 90PVA10OP-S

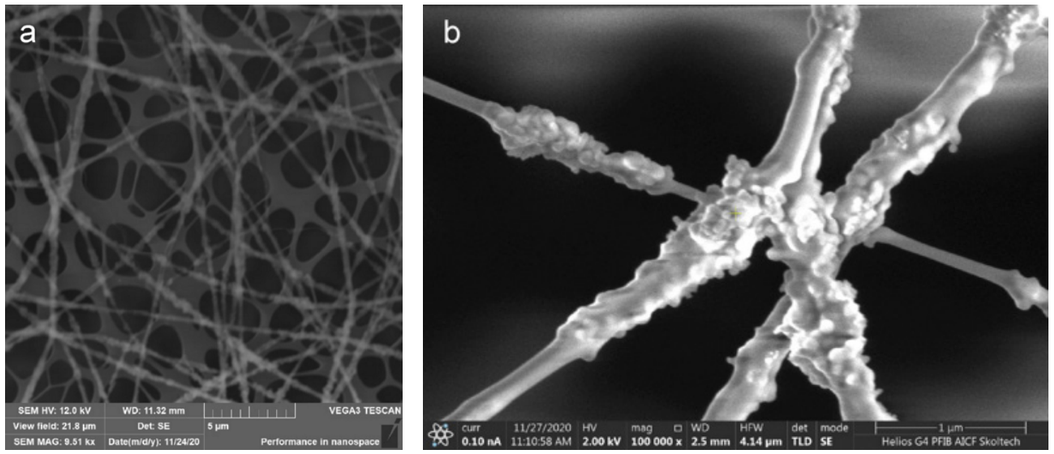

Fig. 3. SEM imaging of morphology 85PVA15OP-S

The distribution of fibrous mat is shown in Fig. 3a, where the 85PVA15OP-S was sputtered on the top of copper grid for TEM. The size of fibers was varied from 115 nm to 230 nm. Some aggregates were clearly observed, but due to the low conductivity of the polymer composite, SEM analysis was not informative enough to identify the specific features of the nanoparticles. Thus, the sample should be characterized by additional methods to study the effect of nanoparticles in future studies. The TEM was therefore implemented to study nanoparticles in fibers obtained by electrospinning. This is one of the most effective methods for detecting the distribution of nanoparticles across fibers. High-resolution fiber images allow us to calculate the average size of nanoparticles and perform Energy Dispersive X-Ray (EDX) mapping of chemical elements.

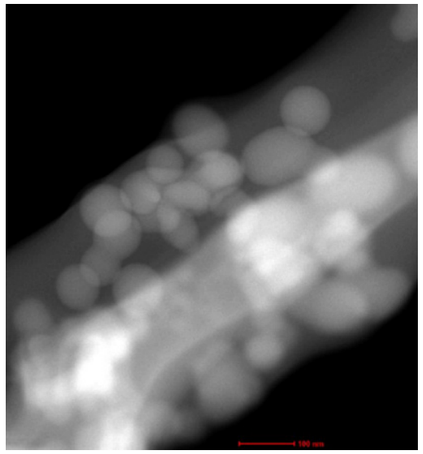

Fig. 4. STEM image of 90PVA10OP-S

STEM imaging of polymer composite afforded to visualize the embedded nanoparticles of SiO_2 within the depth of nanofiber. Mean size of nanoparticles was 76 ± 30 nm in Fig. 4. The EDX analysis (Fig. 5) showed that the chemical mapping of Si was distributed in depth of nanofiber. The mapping of chemical elements proves the clear presence of silica agglomerates.

The electrospinning of polymers promotes a fiber as a building block for a three-dimensional fibrous membrane separator. The concept of hierarchically organized materials includes the processing of materials with scaled structure and morphology. Nanofibers were successfully produced in the laboratory set up of electrospinning by Fablab.

Moreover, the synergetic effect was available due to the electrospun components in one solution. The polyvinyl alcohol was proven as a stable component to support the electrospinning in a given PVA/OP-S solutions. In this ongoing research, we have managed to obtain the silica nanoparticles embedded in PVA fibers. Challenges still exist for the use of the obtained experience to design multilayered composites.

V. CONCLUSIONS

In this article, we proved the electrospinability of PVA based solutions. The electronic microscopy indicated the high performance of using the PVA 10 wt.% as a binding solution in compounds. The host polymer provided the repetitive electrospinning process, whereas the additive components were embedded in the structure to enrich the fiber properties. The agglomerates occurred since the overloading of silica solution (10-15 wt.%) resulted in the bead formation on fibers. Thus, we identified the need to reduce the fraction of silica content in our composite.

The further stage of research will focus on studying the mechanical characteristics and wettability of the obtained material. We plan to conduct the tensile testing using the Deben microtesting machine (UK) and to measure electrolyte wettability using contact angle method.

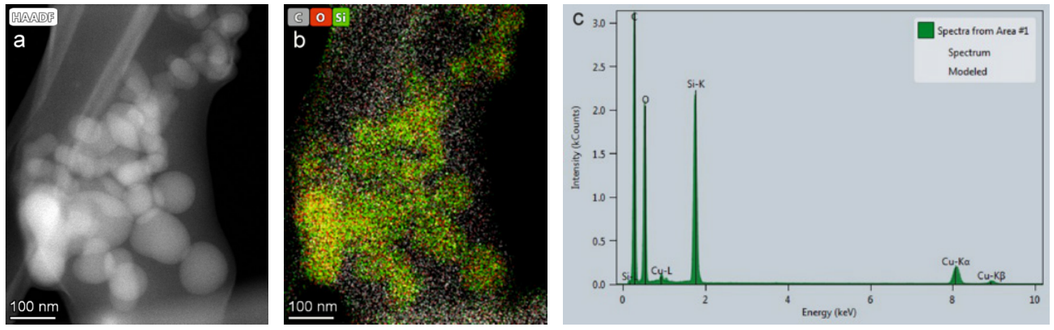

Fig. 5. TEM images of fibers 90PVA10OP-S

VI. ACKNOWLEDGEMENTS

Author thanks the Center for Energy Storage and Technology and FabLab and Machine Shop Shared Facility for the support and guidance of this project. Especially authors would like to thank the staff of Advanced Imaging Core Facility: Dr. Svetlana Lipovskikh and Dr. Maria Kirsanova for their help.

VII. REFERENCES

[1] S. Ma et al., "Temperature effect and thermal impact in lithium-ion batteries: A review," *Progress in Natural Science: Materials International*, vol. 28, no. 6, pp. 653–666, 2018.

[2] Z. Lu et al., "Polyimide separators for rechargeable batteries," *Journal of Energy Chemistry*, vol. 58, pp. 170–197, 2021.

[3] "Battery Separator Materials Market - Global Industry Analysis and Forecast 2026." [Online]. Available: https://www.transparencymarketresearch.com/battery-separator-materials-market.html. [Accessed: 16-Mar-2021].

[4] "Celgard® High Performance Battery Separators." [Online]. Available: www.Celgard.com. [Accessed: 13-May-2021].

[5] H. Zhang, M. Y. Zhou, C. E. Lin, and B. K. Zhu, "Progress in polymeric separators for lithium ion batteries," *RSC Advances*, vol. 5, no. 109, pp. 89848–89860, 2015.

[6] A. A. Heidari and H. Mahdavi, "Recent Development of Polyolefin-Based Microporous Separators for Li–Ion Batteries: A Review," *Chemical Record*, vol. 20, no. 6, pp. 570–595, 2020.

[7] E. Wang, C. H. Chiu, and P. H. Chou, "Safety assessment of polyolefin and nonwoven separators used in lithium-ion batteries," *J. Power Sources*, vol. 461, p. 228148, 2020.

[8] Y. S. Chung, S. H. Yoo, and C. K. Kim, "Enhancement of meltdown temperature of the polyethylene lithium-ion battery separator via surface coating with polymers having high thermal resistance," *Ind. Eng. Chem. Res.*, vol. 48, no. 9, pp. 4346–4351, 2009.

[9] Y. Li, Q. Li, and Z. Tan, "A review of electrospun nanofiber-based separators for rechargeable lithium-ion batteries," *Journal of Power Sources*, vol. 443, p. 227262, 2019.

[10] H. Cai et al., "Electrospun polyethylene terephthalate nonwoven reinforced polypropylene separator: Scalable synthesis and its lithium ion battery performance," *Polymers (Basel)*, vol. 10, no. 6, p. 574, 2018.

[11] J. R. Kim, S. W. Choi, S. M. Jo, W. S. Lee, and B. C. Kim, "Electrospun PVdF-based fibrous polymer electrolytes for lithium ion polymer batteries," *Electrochim. Acta*, vol. 50, no. 1, pp. 69–75, 2004.

[12] F. Khodaverdi, A. Vaziri, M. Javanbakht, and M. Jahanfar, "Improvement of PAN separator properties using PVA/malonic acid by electrospinning in lithium ion-batteries," *J. Appl. Polym. Sci.*, vol. 138, no. 13, p. 50088, 2021.

[13] M. Yanilmaz, "Evaluation of electrospun PVA/SiO_2 nanofiber separator membranes for lithium-ion batteries," *J. Text. Inst.*, vol. 111, no. 3, pp. 447–452, 2020.

[14] H. Widiyandari, A. Purwanto, and S. A. Widyanto, "Polyvinilidine fluoride (PVDF) nanofiber membrane for Li-ion rechargeable battery separator," *J. Phys. Conf. Ser.*, vol. 817, no. 1, p. 012013, 2017.

[15] R. Arthi, V. Jaikumar, and P. Muralidharan, "Development of electrospun PVdF polymer membrane as separator for supercapacitor applications," *Energy Sources, Part A Recover. Util. Environ. Eff.*, p. 1649746, 2019.

[16] S. Park et al., "Multicore-shell nanofiber architecture of polyimide/polyvinylidene fluoride blend for thermal and long-term stability of lithium ion battery separator," *Sci. Rep.*, vol. 6, p. 36977, 2016.

[17] K. Li, X. Liu, Y. Liu, and X. Wang, "A piezoelectric generator based on PVDF/GO nanofiber membrane," in *J. Phys. Conf. Ser.*, vol. 1052, no. 1, p. 12110, 2018.

[18] L. Yan, Y. S. Li, C. B. Xiang, and S. Xianda, "Effect of nano-sized Al_2O_3-particle addition on PVDF ultrafiltration membrane performance," *J. Memb. Sci.*, vol. 276, no. 1–2, pp. 162–167, 2006.

[19] L. Yao, T. W. Haas, A. Guiseppi-Elie, G. L. Bowlin, D. G. Simpson, and G. E. Wnek, "Electrospinning and stabilization of fully hydrolyzed poly(vinyl alcohol) fibers," *Chem. Mater.*, vol. 15, no. 9, pp. 1860–1864, 2003.

[20] W. Xiao, J. Song, L. Huang, Z. Yang, and Q. Qiao, "PVA-ZrO_2 multilayer composite separator with enhanced electrolyte property and mechanical strength for lithium-ion batteries," *Ceram. Int.*, vol. 46, no. 18, pp. 29212–29221, 2020.

[21] M. J. Uddin, P. K. Alaboina, L. Zhang, and S. J. Cho, "A low-cost, environment-friendly lignin-polyvinyl alcohol nanofiber separator using a water-based method for safer and faster lithium-ion batteries," *Mater. Sci. Eng. B Solid-State Mater. Adv. Technol.*, vol. 223, pp. 84–90, 2017.

[22] M. R. Asghar, M. T. Anwar, A. Naveed, and J. Zhang, "A review on inorganic nanoparticles modified composite membranes for lithium-ion batteries: Recent progress and prospects," *Membranes*, vol. 9, no. 7, p.78, 2019.

[23] S. K. Tiwari and S. S. Venkatraman, "Importance of viscosity parameters in electrospinning: Of monolithic and core-shell fibers," *Mater. Sci. Eng. C*, vol. 32, no. 5, pp. 1037–1042, 2012.

Small reviews

Linear Ion Traps

Timur Abbasov*, Ivan Sherstov, Arkadi Shipulin

Abstract **Nowadays, trapped ions are a very promising architecture in various applications: from mass spectrometry to frequency standards and quantum simulations. In this article, we summarized how ions can be stored in some area and present a brief review of different constructions of the linear ion traps.**

Index Terms **Frequency standard, ion, linear ion trap, surface trap.**

I. INTRODUCTION

THE first experiments with trapped ions were conducted more than 60 years ago [1]-[3], and a lot of studies with stored charged particles were made since then [4]-[9]. There are a lot of different applications for frequency standards. Except for the timekeeping, the resolution of global navigation systems like GPS, GLONASS, and GALILEO rely on the stability of onboard atomic clocks. Moreover, precise frequencies can be used for a more accurate definition of physical units.

There are two main divisions in frequency standard research with trapped particles: a system with trapped neutral atoms and a system with charged ions. Each approach has its advantages and disadvantages. In systems with neutral atoms, there are a lot of particles in the working area. Therefore, there is an excellent signal-to-noise ratio. However, systems with trapped charged ions are more stable because of the huge lifetime of the ion in a trap.

The working principle of the ion frequency standards is based on the quantum-jump spectroscopy of the narrow “clock” transition of the trapped ion. Such an approach is described in many works [4]-[6]. Clock transitions exist in a large number of different ions. The most promising ions are $^{171}Yb^{+}$, $^{88}Sr+$, $^{43}Ca+$, $^{199}Hg+$, and $^{115}In+$ [4]-[7], not only because of the transitions that can be used as frequency standards but also because they can be manipulated with convenient laser wavelengths.

Since the first demonstration of a single trapped ion in 1980, experiments with trapped single particles have led to some of the finest spectroscopic measurements in physics [8], [9] and radiofrequency (RF) Paul traps have become excellent working tools with unsurpassed accuracy in frequency metrology [4], [5].

Modern technologies are capable of producing compact RF ion traps. While the size of the frequency standard components (vacuum chambers, pumps, lasers, etc.) is constantly decreasing, it has become possible to create very compact, transportable, and highly accurate frequency standards for different airborne or even space applications. Such precise and portable systems

T. Abbasov is with Center for Photonics and Quantum Materials, Skolkovo Institute of Science and Technology, Skolkovo Innovation Center, Building 3, Moscow 121205, Russia (e-mail: timur.abbasov@skoltech.ru).
I. Sherstov is with Center for Photonics and Quantum Materials, Skolkovo Institute of Science and Technology, Skolkovo Innovation Center, Building 3, Moscow 121205, Russia.
A. Shipulin is with Center for Photonics and Quantum Materials, Skolkovo Institute of Science and Technology, Skolkovo Innovation Center, Building 3, Moscow 121205, Russia.

are sensitive to gravitational heterogeneities and can find oil and gas fields and among other things. Also, trapped ions are promising candidates to use in quantum computation systems. Their long coherence times, state initialization and detection, and precisely controllable and versatile interactions make them excellent systems for quantum simulation experiments.

II. ION TRAPPING MECHANISM

To store an ion in some volume, we need to create a stable balance condition for the ion in this volume. It means that if ion moves from some point, it experiences a restoring force that pushes it back to the stable region.

The most common analogy of this process is an example with an ideal zero-length spring connected to the trapping point from one side and to the ion from another side. In the anisotropic situation, the energy potential could be written as:

$$U(x, y, z)=\frac{1}{2}(\alpha x^2+\beta y^2+\gamma z^2) \quad (1)$$

To store a charged particle, we can create an electric potential:

$$\Phi(x, y, z)=U/Q=\frac{1}{2Q}(\alpha x^2+\beta y^2+\gamma z^2) \quad (2)$$

where Q is an electrical charge of the particle. The Laplace equation in this situation looks like $\Delta\Phi=\alpha+\beta+\gamma=0$. It means that at least one of the coefficients should be negative. Such potential presents a saddle point with "anti-trapping" force in at least one direction. Therefore, a static electric field cannot be used for charged particle trapping.

One of the ways to solve this problem is to use RF electric potentials and periodically rotate a saddle point as shown in Fig. 1. In this situation, the motion of the ion can be decomposed into two motions: micromotion and secular motion. The first one is small in amplitude and driven by the RF field, and the second one is slower but bigger in amplitude. The time-averaged force, which the ion experiences in such a field, can be trapping in every direction under some conditions. According to the Paul trap theory [10], **[11]**, such a force can be described in terms of pseudopotential:

$$\Psi(x, y, z)=\frac{Q}{4M\Omega^2}|\nabla\Phi(x, y, z)|^2 \quad (3)$$

where Ω is an angular frequency of the RF field and M is the mass of the particle.

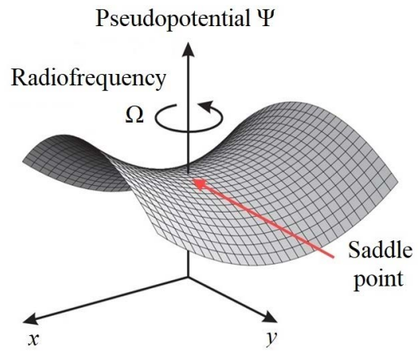

Fig. 1. The potential surface of a quadrupole trap with hyperbolically shaped electrodes with a saddle point

As $E(x, y, z)=-\nabla\Phi(x, y, z)$, the potential increases as the square of the magnitude of the electric field. It means that the minimum of the potential (the trapping point) will be located in the field node. The energy potential can be approximated with a harmonic potential near this point.

III. IDEAL TRAP

The ideal linear quadrupole ion trap consists of electrodes with such a configuration that the electric field can be written using (2) with coefficients $\alpha=-\beta=QV/R^2$ and $\gamma=0$.

Such a potential can be generated with four hyperbolically shaped electrodes with a distance 2R between the opposite electrodes and by applying opposite voltages $\pm V/2$, as shown in Fig. 2.

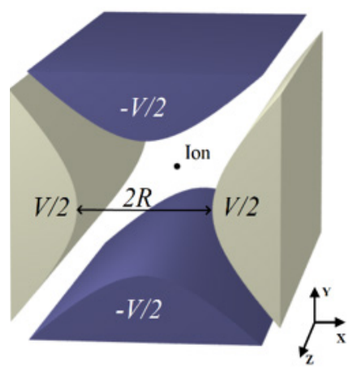

Fig. 2. The ideal Paul trap with four hyperbolically shaped electrodes. A potential difference between each pair of neighboring electrodes is V [11].

By using an RF voltage, we can trap ions as described above. In practice, it is more convenient to apply $V(t)=V_{DC}+V_{RF}\cos(\Omega t)$ to the first pair of opposite electrodes and keep the other pair of electrodes in the ground potential (GND). Here V_{RF} is the amplitude of the RF voltage and V_{DC} is the applied DC voltage.

For such a configuration, equations of motion for the trapped ion take a simple form:

$$\ddot{x}=-\frac{Qx}{MR^2}V(t) \quad \text{and} \quad \ddot{y}=-\frac{Qy}{MR^2}V(t).$$

These differential equations are a case of the known Mathieu equations with the stability parameters a and q:

$$a=\frac{4QV_{DC}}{MR^2\Omega^2} \quad q=\frac{2QV_{RF}}{MR^2\Omega^2}.$$

Using these parameters, we can define regions of stable trapping, where the ion trajectories are bounded.

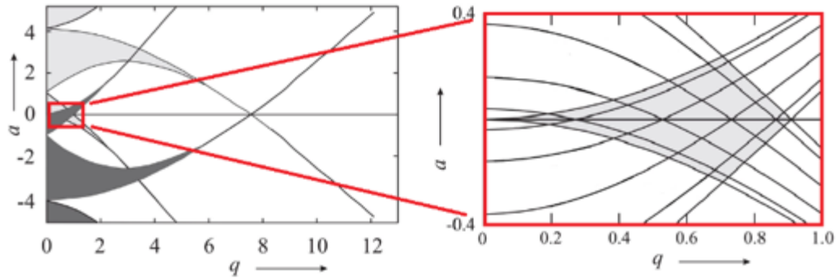

Fig. 3. Stability diagram with a and q parameters (left) and the first region of stable trapping (right) [7].

For practical purposes, the most important region is the first one with the lowest parameters q and a.

IV. NON-IDEAL TRAPS

A. Rod-shaped trap

In practice, it is more convenient to use rod-shaped electrodes instead of hyperbolically shaped ones [12], [13], as shown in Fig. 4.

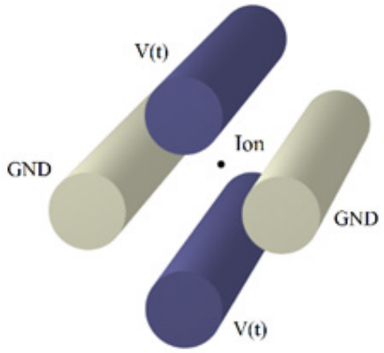

Fig. 4. Four rod-shaped electrodes geometry of a linear Paul trap [11].

Such a configuration is used for different variety of applications. For axial ion confinement and better ion manipulations, ring electrodes [14], segmented rod electrodes [15], or endcap electrodes [16] can be used. The first two variants are shown in Fig. 5.

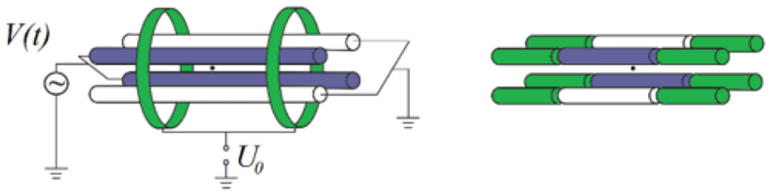

Fig. 5. Linear rod-shaped Paul traps with additional ring electrodes (left) and segmented electrodes (right) for the axial confinement of the ion [7].

The main advantage of using such a configuration is the simplicity of the construction. It is easy to calculate, fabricate and operate. Unfortunately, it has drawbacks, such as big geometry dimensions and poor optical access to the stored ions.

Different attempts were made to decrease trap dimensions, provide better optical access to the stored ions, simplify the manufacturing process, and improve some trapping parameters. These traps have different shapes of potentials, which can be non-harmonic. However, near the field node, the physics remains the same as before. Ion traps are usually made with a gold layer on top of the electrode surface to decrease the influence of the black-body radiation shift on the width of the ion transitions. For better adhesion of the gold, the body of the electrodes can be made from titanium.

B. Blade trap

One of the examples of the design improvements is the "blade trap" [17]. It consists of four blade electrodes which are held together with a special mount. Each blade is split into five segments connected on the RF blades and isolated from each other on the static ones.

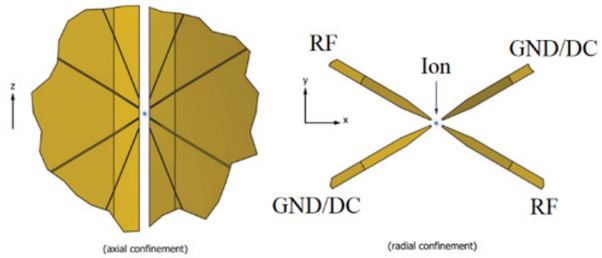

Fig. 6. Schematic representation of the linear Paul trap with four blade-shaped electrodes [17].

This type of ion trap can be much more compact compared to the trap with rod-shaped electrodes and provides better optical access to the stored ions. Segmentation of the electrodes allows controlling trapped ions independently from each other and generating an axially confining potential.

C. Multi-Layer Trap

Another example of a different ion trap design is a multi-layer trap with several electrodes aligned in several layers. An example of such a trap is shown in Fig. 7. It consists of three layers of segmented electrodes and was created in PTB Germany for quantum simulations [18].

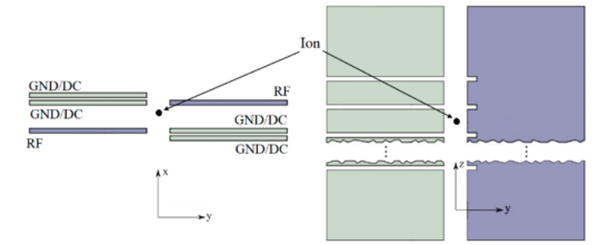

Fig. 7. Schematic representation of the linear Paul trap with electrodes located in several layers. Left: side view, right: top view [18].

Multi-layer traps can be created using technologies from the semiconductor industry, such as lithography, plasma etching, and physical vapor deposition [19], [20]. Thus, such a construction can be created without any manual assembly and with a sub-μm resolution.

D. Surface trap

One of the most promising architectures for a compact Paul trap is a chip-based surface trap with electrodes in one plane. First ion traps with electrodes in one plane were tested at NIST in 2006 [21]. Such architecture also has the advantage of optical access to the stored ion because ions are trapped above the surface of the trap. It helps to direct radiation from different laser systems into the ion and detect the stored ion with higher probability. Such an architecture also allows using elements of integrated photonic circuits [22] which helps minimize the whole system dimensions and makes it more stable to external impacts.

A huge amount of surface traps has been built since then to improve various characteristics. In order to improve the fabrication process and trap performance, a lot of different materials for substrate and electrodes have been tested [23], [24]. Eventually, the fabrication of surface traps was combined with well-known silicon-pattering technologies [25]. It significantly helped improve the resolution of narrow regions on a trap and made the planar trap production much more convenient.

A typical realization of such a surface trap is described in several theses [10], [11] and is shown in Fig 8.

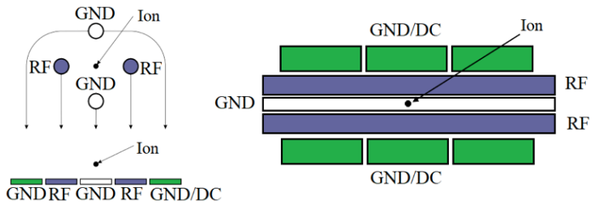

Fig. 8. Planar ion trap as a result of "deformation" of the rod electrodes into the surface electrodes from a side view (left) and top view (right).

A stripe of a ground electrode is located between two also stripe-shaped RF electrodes. Segmented electrodes on both sides of the RF electrodes are applied with DC voltage and serve for the ions' confinement in the axial direction and compensate the ions' secular motions. All electrodes are located on top of the dielectric substrate.

V. CONCLUSION

In conclusion, we demonstrated the theory of the ion trapping process and showed the most popular linear Paul trap designs. All these designs are different versions of the ideal Paul trap with hyperbolically-shaped electrodes created to improve some trapping parameters, make manipulations with the stored ions easier, and improve the trap fabrication process. Despite the significant change of the whole trap geometry, physics near the trapping region remains the same, and calculations of different trap parameters can be adapted to the new geometry without profound changes.

VII. REFERENCES

[1] W. Paul, O. Osberghaus, and E. Fischer, *An ion cage*. Wiesbaden, Germany: VS Verlag für Sozialwissenschaften, 1958.

[2] R. F. Wuerker, H. Shelton, and R. V. Langmuir, "Electrodynamic containment of charged particles," *J. Appl. Phys.*, vol. 30, no. 3, pp. 342–349, 1959.

[3] E. Fischer, "The three dimensional stabilization of charge carriers in a [rf. electric] quadrupole field," *Eur. Phys. J. A*, vol. 156, no. 1, pp. 1–26, 1959.

[4] T. Rosenband et al., "Frequency ratio of Al+ and Hg+ single-ion optical clocks; metrology at the 17th decimal place," *Science*, vol. 319, no. 5871, pp. 1808–1812, 2008.

[5] C. W. Chou, D. B. Hume, J. C. J. Koelemeij, D. J. Wineland, and T. Rosenband, "Frequency comparison of two high-accuracy Al+ optical clocks," *Phys. Rev. Lett.*, vol. 104, no. 7, p. 070802, 2010.

[6] P. Gill et al., "Trapped ion optical frequency standards," *Meas. Sci. Technol.*, vol. 14, no. 8, pp. 1174–1186, 2003.

[7] F. Riehle, *Frequency Standards: Basics and Applications*. Weinheim, Germany: Wiley-VCH Verlag, 2006.

[8] W. Neuhauser, M. Hohenstatt, P. Toschek, and H. Dehmelt, "Optical-sideband cooling of visible atom cloud confined in parabolic well," *Phys. Rev. Lett.*, vol. 41, no. 4, pp. 233–236, 1978.

[9] G. Werth, V. N. Gheorghe, and F. G. Major, *Charged particle traps II*. Berlin, Heidelberg: Springer Berlin Heidelberg, 2009.

[10] D. Niedermayr, "Cryogenic surface ion traps," Ph.D. dissertation, University of Innsbruck, Innsbruck, 2015.

[11] C. E. Pearson, "Theory and Application of Planar Ion Traps," Ph.D. dissertation, University of Washington, Seattle, 2006.

[12] D. A. Church, "Storage-ring ion trap derived from the linear quadrupole radio-frequency mass filter," *J. Appl. Phys.*, vol. 40, no. 8, pp. 3127–3134, 1969.

[13] I. Waki, S. Kassner, G. Birkl, and H. Walther, "Observation of ordered structures of laser-cooled ions in a quadrupole storage ring," *Phys. Rev. Lett.*, vol. 68, no. 13, pp. 2007–2010, 1992.

[14] D. J. Berkeland, J. D. Miller, J. C. Bergquist, W. M. Itano, and D. J. Wineland, "Laser-cooled mercury ion frequency standard," *Phys. Rev. Lett.*, vol. 80, no. 10, pp. 2089–2092, 1998.

[15] M. G. Raizen, J. M. Gilligan, J. C. Bergquist, W. M. Itano, and D. J. Wineland, "Ionic crystals in a linear Paul trap," *Phys. Rev. A*, vol. 45, no. 9, pp. 6493–6501, 1992.

[16] P. T. H. Fisk, M. J. Sellars, M. A. Lawn, C. Coles, A. G. Mann, and D. G. Blair, "Performance of a prototype microwave frequency standard based on trapped 171Yb+ ions," in *Proceedings of IEEE 48th Annual Symposium on Frequency Control*, 2002.

[17] K. G. Johnson, "Experiments with Trapped Ions and Ultrafast Laser Pulses," Ph.D. dissertation, University of Maryland, Maryland, 2016.

[18] N. Herschbach, K. Pyka, J. Keller, and T. E. Mehlstäubler, "Linear Paul trap design for an optical clock with Coulomb crystals," *Appl. Phys. B*, vol. 107, no. 4, pp. 891–906, 2012.

[19] G. Wilpers, P. See, P. Gill, and A. G. Sinclair, "A monolithic array of three dimensional ion traps fabricated with conventional semiconductor technology," *Nature Nanotechnology*, vol. 7, p. 572 6, 2012.

[20] D. Stick, "Ion trap in a semiconductor chip," *Nature Physics*, vol. 2, p. 36 39, 2005.

[21] S. Seidelin et al., "Microfabricated surface-electrode ion trap for scalable quantum information processing," *Phys. Rev. Lett.*, vol. 96, no. 25, p. 253003, 2006.

[22] K. R. Brown, J. Kim, and C. Monroe, "Co-designing a scalable quantum computer with trapped atomic ions," *Npj Quantum Inf.*, vol. 2, no. 1, p. 16034, 2016.

[23] N. Daniilidis et al., "Corrigendum: Fabrication and heating rate study of microscopic surface electrode ion traps," *New J. Phys.*, vol. 14, no. 7, p. 079504, 2012.

[24] S. X. Wang, Y. Ge, J. Labaziewicz, E. Dauler, K. Berggren, and I. L. Chuang, "Superconducting microfabricated ion traps," *Appl. Phys. Lett.*, vol. 97, no. 24, p. 244102, 2010.

[25] J. Britton, D. Leibfried, J. A. Beall, R. B. Blakestad, J. H. Wesenberg, and D. J. Wineland, "Scalable arrays of rf Paul traps in degenerate Si," *Appl. Phys. Lett.*, vol. 95, no. 17, p. 173102, 2009.

Carbon Nanotube/Polymer Composites as Sensor Materials

Ilya V. Novikov*, Fedor S. Fedorov, Albert G. Nasibulin

Abstract **Due to their unique properties (electrical conductivity, mechanical properties, large surface area and aspect ratio), carbon nanotubes (CNTs) are of great interest and are widely used as a reinforcing agent in polymer nanocomposites. However, in addition to improving the mechanical properties, such composites can be utilized in a number of other more complex applications as a highly functional material, such as stretchable electronics, energy storage devices, biomedicine, sensor materials, and many others. In this review, we focus on CNT/polymer composites for sensor devices. Herewith, we will consider both mechanical and chemical sensors, discuss the general principles of their operation, and highlight the latest achievements of researchers in this area.**

Index Terms **Carbon nanotubes, carbon nanotube/polymer composites, chemical sensors, mechanical sensors.**

I. NOMENCLATURE

R	resistance (Ω)
l	length (mm)
ε	strain (mm/mm)
R_{CNT}	intrinsic resistance of carbon nanotubes (Ω)
R_c	resistance between carbon nanotubes that are physically in contact (Ω)
R_t	tunneling resistance between carbon nanotubes (Ω)
s	gap between carbon nanotubes (Å)
K	average height of the potential barrier (eV)

* Ilya V. Novikov is with the Center of Photonics and Quantum Materials, Skolkovo Institute of Science and Technology, Skolkovo Innovation Center, Building 3, Moscow 121205, Russia (e-mail: ilya.novikov@skoltech.ru).
Fedor S. Fedorov is with the Center of Photonics and Quantum Materials, Skolkovo Institute of Science and Technology, Skolkovo Innovation Center, Building 3, Moscow 121205, Russia (e-mail: f.fedorov@skoltech.ru).
Albert G. Nasbulin is with the Center of Photonics and Quantum Materials, Skolkovo Institute of Science and Technology, Skolkovo Innovation Center, Building 3, Moscow 121205, Russia (e-mail: a.nasibulin@skoltech.ru).

II. INTRODUCTION

FOR nearly three decades, CNT/polymer composites have attracted the attention of researchers because of excellent combination of mechanical, electrical, and thermal properties and have been investigated intensively [1]. One of the first significant works on the synthesis of composites based on CNTs and polymers dates back to 1994 [2]. Ajayan et al. obtained aligned multi-walled CNTs (MWCNTs) in epoxide-based resin by mechanical mixing and subsequent hardening of composite upon exposure at elevated temperature. Since then, many advanced methods for fabrication of CNT-based polymer composites have been proposed as well as lots of unique properties of such composites have been revealed and studied. The one is the sensitivity of polymer composites with loaded carbon nanotubes towards mechanical or chemical perturbations. Indeed, CNT/polymer composites have been found to have a response to various external stimuli, such as strain, pressure, gases, chemical vapors, temperature, and many others [3]. Furthermore, in the vast majority of cases, the response is resistive. This means that under external influences, for example, mechanical or chemical, the resistance of the composite changes.

The general principle of these phenomena is associated with the structural features of the composites. Essentially, polymer nanocomposite is a polymer matrix with embedded nanofillers. In the case of CNT/polymer composites, the fillers are conductive carbon nanotubes, which form a conductive 3D network above the critical concentration called percolation threshold. Under the external influence, the average distance between nanotubes may be altered causing the change in the number of intertube junctions. This leads to crucial changes in overall resistance of the composite, since tunneling through dielectric polymer from one nanotube to another one depends exponentially on the distance between them.

In what follows, we will touch upon the two most intensively studied areas of sensors based on CNT/polymer composites, namely, mechanical (primarily strain) and chemical sensors.

III. AN OVERVIEW OF CNT/POLYMER SENSORS

A. CNT/polymer composites as mechanical sensors.

Mechanical sensors are widely used in the engineering fields for damage detection as well as for material structure characterization. Traditional strain gauges based on metals or semiconductors (primarily silicon) possess certain drawbacks, in particular, quite low resolution in nanoscale and a principle possibility to perform measurements only in a specific direction. The fiber Bragg grating (FBG) sensors are quite promising optical fibers sensors. Although they demonstrate good strain sensing characteristics and are capable to withstand very high strain, FBG strain sensors are insensitive at a nanoscale [4]. In this regard, alternative approaches for fabrication of strain gauges that could work at the nanoscale and in all directions of tension, as well as demonstrate high elasticity, have begun to be developed actively in recent years. Because of their ease of manipulation, chemical versatility, unique electrical and mechanical properties carbon nanomaterials have attracted great attention as a promising alternative materials to existing prototypes [5]. To date, there are works on strain sensors, in which graphene, carbon nanotubes, carbon black, and carbon nanofibers have been used as functional materials. Graphene-based strain sensors show the greatest sensitivity; however, they are beyond of the scope of the present review and, for interested readers, we recommend the comprehensive review by Yee et al. [5].

CNT-based strain sensors are divided into two groups, which are CNT films (often called in the literature as buckypapers) and CNT/polymer composites. Early investigations were mostly related to the films based on single-walled CNTs (SWCNTs). SWCNTs are essentially a sheet of graphene rolled up at a certain chiral angle – a monoatomic two-dimensional honeycomb crystal lattice of carbon. However, SWCNTs may be either metallic or semiconducting since they are strongly chirality-dependent; therefore, the trend of the fabrication of strain sensors switched to the utilization of multi-walled CNTs (MWCNTs).

Although CNT films have exhibited relatively high sensing performance, recently, more attention has been paid to the CNT/polymer composites. This is associated mainly with the ability to successfully detect large strain deformations, reaching several hundred percent. Various polymers have been considered, including polystyrene (PS), poly(methyl methacrylate) (PMMA),

polyvinyl alcohol (PVA), epoxy resin, and many others. At the same time, elastomer-based sensors are most interesting and promising materials as displaying high elasticity, which means low Young's modulus and relatively high tensile strength. Due to this feature, elastomer-based strain sensors are capable of operating at very high strains.

Before the consideration of some works on CNT/polymer composite-based mechanical sensors, let us first consider the fundamental mechanisms of operation of such sensors. Sensitivity of CNT/polymer composites is related to the piezoresistive properties of the network of carbon nanotubes within the polymer matrix. It should be noted here that we are not talking about the classical piezoelectric effect caused by the polarization of the dielectric under the action of external forces. The piezoresistivity of composites should be taken in an integral sense, as a change in resistance at tensile strength. To characterize the magnitude of this effect, that is, the sensitivity of the strain sensor, gauge factor (GF) is used, which is determined by the ratio of the relative change in resistance to the relative elongation (strain):

$$GF = \frac{\Delta R/R}{\Delta l/l} = \frac{\Delta R/R}{\varepsilon}. \quad (1)$$

In a nanotube network, two types of resistance can be distinguished: the intrinsic resistance of nanotubes (RCNT, "intra-CNT" resistance) and the resistance of inter-tube contacts ("inter-CNT" resistance) (Fig. 1). In this case, the resistance between nanotubes is divided into the contact resistance (Rc, when two nanotubes are in physical contact) and tunneling resistance (Rt, when there is a small gap between nanotubes). In sensors based on CNT films, the intrinsic resistance is important, since it increases significantly even at low loads [4]. However, the contact resistance between the tubes prevails over the internal resistance. This is due to the Schottky barrier at tube-to-tube junctions within the network. It significantly depends on the contact area, hence, the diameter of the nanotubes, as well as on the nature of the nanotubes [6]. In polymer composites, the first two contributions are of lesser importance. Since, as a rule, the concentration of nanotubes in the polymer does not exceed a few percent, the stretching of the composite sample occurs due to the elongation of the polymer chains. This leads to an increase in the average distance between nanotubes. As it was mentioned above, tunneling resistance depends exponentially on the distance between CNTs:

$$R_t = R_0 e^{\lambda s}, \quad (2)$$

where R_0 and λ may be expressed as follows (assuming small bias voltage and rectangular barrier K):

$$R_0 = \frac{1}{C_1}\frac{s}{\sqrt{K}}; \lambda = C_2\sqrt{K} \quad (3)$$

with the constants C_1 = 3.16 x 10^{10}, C_2 = 1.0125 [4]. Thus, at relatively low strains (within elasticity region), change in resistance may be considerable, resulting in high values of GF.

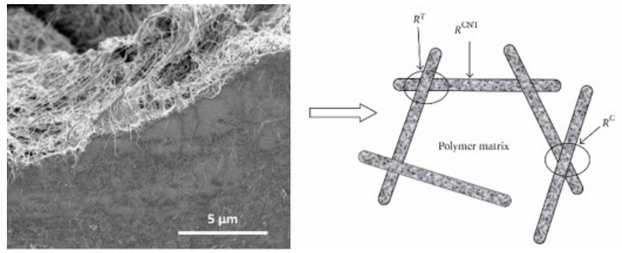

Fig. 1. Typical SEM image of the CNT/polymer composite (left); representation of CNT network in a polymer matrix [4].

One of the first key works on CNT/polymer composites used a strain sensor was published in 2006 by Kang et al. [7]. They fabricated SWCNT/PMMA composite film by casting the suspension of SWCNTs in PMMA solution in a teflon mold followed by curing in a vacuum oven at room temperature. They compared the performance of such composite film with buckypaper of SWCNTs and found noticeable advantages of composite films. This was mainly attributed to the relatively weak van der Waals attractions between nanotubes causing their slippage and degradation of the network allowing performance only within the range of 500 microstrain. Despite lower sensitivity compared to buckypaper sensor, there are strong polymer interfacial bindings. This leads to the improvement of strain transfer across the CNT/PMMA sensor. Also linear reversible strain response under static and dynamic strain tests has been shown. In another significant early study [8], Zhang et al. investigated CNT/elastomer strain sensor performance. They showed good agreement with prevailing tunneling mechanism of the change in CNT network conductivity within the elastomer matrix by demonstration of universal concentration-independent exponential relationship between resistivity and strain. However, for lower (0-5%) strains, the resistivity-strain dependence was explained by the deformation of the conductive network. In their following paper [9], these authors considered recoverability and reproducibility of such composite-based sensors by cycling loading and found good performance at small amplitudes, while at larger strains, only a small part of resistance is recoverable. This was attributed to the competing processes of network deformation and network reformation during cyclic loading.

In more recent works, researchers have used more diverse methods of fabricating composites. Thus, in the work [10], 3D-printed composites based on MWCNTs and thermoplastic polyurethane (TPU) demonstrated a very high GF (about 176). This was caused by high adhesion between printed TPU layers during the fusion process this way providing no degradation of conductivity in both through-layer and cross-layer directions. Thus, in the applications where complex design and customization are demanded, such 3D-printed strain sensors may be employed. In another study [11], the authors fabricated a high-performance lightweight polyurethane-based pressure sensor. This was achieved by the specific inner structure of the composite created by directionally growing ice crystals during synthesis (Fig. 2). This way lightweight composite foam was obtained. Due to the aligned porous structure, such composites exhibited superior piezoresistive behavior. Moreover, the authors showed human motion (such as walk, jump, squat, etc.) detection conducted by such foam pressure sensor.

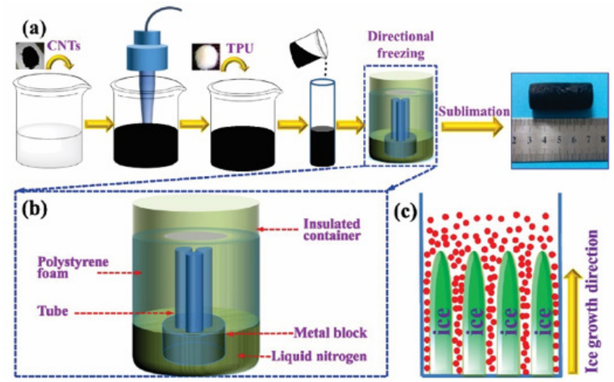

Fig. 2. Fabrication process of the aligned CNT/TPU foam [11].

Thus, CNT/polymer composites are highly effective as a mechanical sensor material. The dominant mechanism of the piezoresistivity of CNT/polymer composites is due to the tunneling resistance between nanotubes, which exponentially depends on the distance between them. However, the deformation and reorganization of a 3D carbon nanotube network in polymer matrix also occurs in a number of cases. The performance of composites can be improved due to better dispersion of the nanotubes in the polymer, as well as by attracting new approaches to the synthesis of composites and the creation of new structures that allow improving the characteristics of the sensor and its applicability in a wide variety of areas.

B. CNT/polymer composites as chemical sensors

Due to the huge specific surface area and conductivity, CNTs are of tremendous interest for chemical sensor applications. Unlike in mechanical sensors, selectivity is a key parameter in a chemical sensor. Although sensitivity and stability are extremely important, in reality, a sensitive sensor unable to distinguish between analytes will essentially produce noise rather than informative signal. Therefore, the task of a chemical sensor is to selectively react to certain external chemical analytes and, based on the received chemical information, convert it into an electrical signal. Many functional materials demonstrate change in resistance by exposure to various vapors and are often called chemiresistors. As with a mechanical sensor, a carbon nanotube-based chemical sensor changes its resistance while being exposed to specific chemical environment.

Other important parameters that characterize sensor performance are drift, response time, recovery time, reversibility, etc. Drift means the response of the sensor in a situation where the environment is not changing. Response time refers to the time sensor takes for an output signal to rise to 90% of its steady state after reacting to an analyte. Conversely, recovery time is the time sensor takes to the signal to fall 10% above the baseline after removing the analyte. Sensor sensitivity is often determined by limit of detection (LOD), which means the minimum concentration of analyte that can be detected at certain confidence level [12]. The illustration of some sensor parameters is presented in Fig. 3.

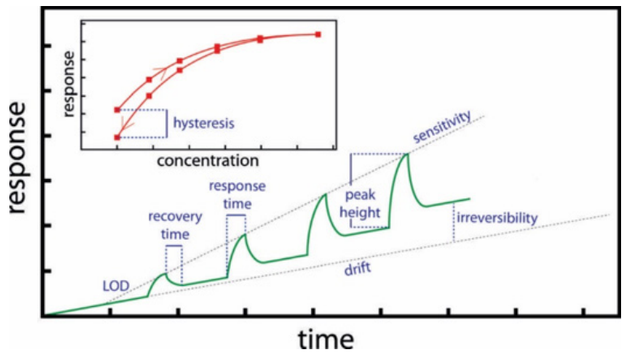

Fig. 3. Representation of sensor performance parameters (at increasing concentration of analyte) [12].

There are three fundamental mechanisms for the operation of sensors based on CNTs. CNT-based sensor responses can be triggered by effects induced within the tube ("intra-CNT", see Fig. 4a). In this case, we are talking about doping CNTs with analytes, which leads to a sharp change in their conductivity. Another type of response is based on the effects arising in the contacts between the CNTs ("inter-CNT", see Fig. 4b), and the third – in the contacts between the CNTs and the electrode (Schottky barrier modulation, see Fig. 4c) [13]. In the case of CNT/polymer composites, this is mainly about the second type of sensing mechanism, namely "inter-CNT" (as in a mechanical sensor).

As was discussed in the previous paragraph, the change in average distance between carbon nanotubes may lead to significant changes in overall composite conductivity. Therefore, the swelling of the polymer matrix leads to a sharp drop in conductivity. Polymer swells in specific analytes, which results in the selectivity of the sensor. The opposite effect can be observed upon drying or destruction (depolymerization) of the polymer under the influence of the analyte, since the disappearance of the non-conductive layer between the tubes leads to the formation of new contacts (Fig. 5). Volumetric changes may be crucially sensitive near the percolation threshold. For this purpose, however, highly uniform spatial distribution of CNTs is required [14].

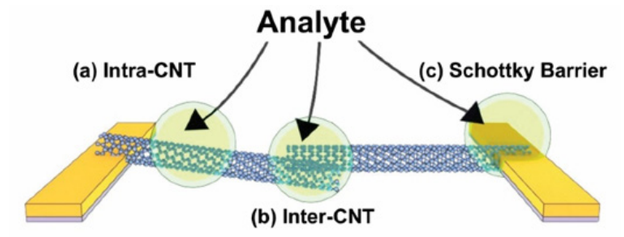

Fig. 4. Different mechanisms of CNT-based chemical sensors [13].

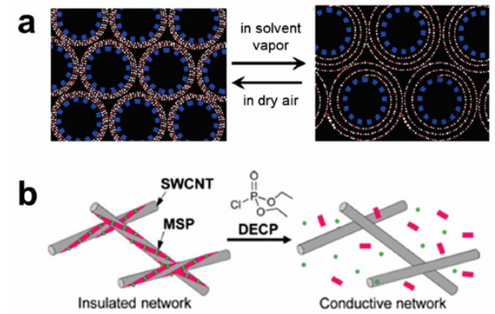

Fig. 5. Illustrations of polymer swelling (a) and polymer decomposition (b) leading to CNT/polymer composite chemiresisitivity (metallosupramolecular polymer (MSP) degrades upon exposure to chemical warfare agent mimic diethyl chlorophosphate (DESP) [13].

Quite common approach relates to covalent functionalization of CNT surface with polymers. This method assumes the growth of selectivity due to the functional groups of polymers. On the other hand, this leads to a partial disruption of nanotube π-electronic structure and, as a consequence, to a decrease in conductivity [13]-[16]. Non-covalent polymer attachment to carbon nanotubes (e.g., physical wrapping) is an alternative type of CNT/polymer composite fabrication, which preserves pristine CNT conductivity; however, the selectivity of such polymers is comparably lower. In one of the pioneer works on CNT/polymer composites as chemical sensors (chemiresistors), Philip et al. [17] compared the performance of PMMA-based composite with pristine MWCNTs and oxidation-modified MWCNTs (o-MWCNTs) and tested sensor responses on various vapors, including dichloromethane, chloroform, acetone, and some others. Both types of composites demonstrated change in resistivity under the specific chemical atmosphere. Yet, the sensitivity of o-MWCNT-based composites appeared to exceed significantly that of pristine MWCNT-based composite sensor. The enhanced response was caused by dipole-dipole interactions between carboxyl group on the CNT surface and the polar organic molecules. Another approach could be fabrication of composites with aligned CNTs. Thus, Wei et al. [18] used an array of aligned nanotubes that were partially coated with polymers along their length (Fig. 6). This approach maintains a high specific surface area of nanotubes, which enhances the sensor sensitivity.

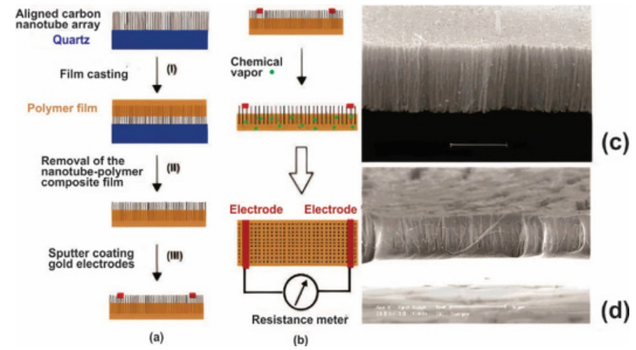

Fig. 6. Scheme of (a) fabrication process (aligned MWCNT synthesis on the quartz substrate; partial covering by polymer film (I); removal of the substrate (II); sputter-coating two strip gold electrodes) and (b) characterizing (monitoring resistance change caused by polymer swelling upon exposure to chemical vapor) the chemical vapor sensor based on polymer composite with aligned CNTs. SEM images of CNT array before (c) and after coating by polymer (d). Scale bar is 5 μm [18].

Nevertheless, the most promising polymers for CNT/polymer composite-based chemical sensors are conductive conjugated polymers, such as polyaniline, polypyrrole, polythiophene, etc. Such polymers combine electronic and magnetic properties of semiconductors and even metals with good mechanical properties and processing advantages typical for polymers. The conductivity changes arise from redox interaction between the polymer and electrically active analytes. This topic is too broad and we direct interested readers to the following reviews [13], [14], [16], [19].

IV. CONCLUSIONS

Summing up, we have considered two main fields of applications of CNT/polymer composites as sensor materials: mechanical and chemical sensors. The principle mechanism of sensor operation is related to the change in the resistivity of CNT network within polymer matrix. Considerable changes in resistance are determined by change in the average distance between carbon nanotubes. In the first case, this displacement is caused by the influence of external force, while in the second one polymer matrix can swell or decompose under the specific chemical environment. Promising results may be achieved by fabricating composites with new artificial structures. Nevertheless, new approaches in CNT organization and functionalization, as well as new effective synthesis methods allowing uniform spatial distribution of CNTs in the polymer will likely determine the development of this technology and may lead to the substitution of most other sensor types.

VII. REFERENCES

[1] G. Mittal, V. Dhand, K. Y. Rhee, S. J. Park, and W. R. Lee, "A review on carbon nanotubes and graphene as fillers in reinforced polymer nanocomposites," *J. Ind. Eng. Chem.*, vol. 21, pp. 11–25, 2015, doi: 10.1016/j.jiec.2014.03.022.

[2] P. M. Ajayan, O. Stephan, C. Colliex, and D. Trauth, "Aligned Carbon Nanotube Arrays Formed by Cutting a Polymer Resin-Nanotube Composite," *Science*, vol. 265, pp. 11–12, 1994, doi: 10.1126/science.265.5176.1212.

[3] A. Kausar, I. Rafique, and B. Muhammad, "Review of Applications of Polymer/Carbon Nanotubes and Epoxy/CNT Composites," *Polym. - Plast. Technol. Eng.*, vol. 55, no. 11, pp. 1167–1191, 2016, doi: 10.1080/03602559.2016.1163588.

[4] W. Obitayo and T. Liu, "A review: Carbon nanotube-based piezoresistive strain sensors," *J. Sensors*, vol. 2012, p. 652438, 2012, doi: 10.1155/2012/652438.

[5] M. J. Yee et al., "Carbon nanomaterials based films for strain sensing application—A review," *Nano-Structures and Nano-Objects*, vol. 18, p. 100312, 2019, doi: 10.1016/j.nanoso.2019.100312.

[6] H. W. Postma, M. de Jonge, Z. Yao, and C. Dekker, "Electrical transport through carbon nanotube junctions created by mechanical manipulation," *Phys. Rev. B - Condens. Matter Mater. Phys.*, vol. 62, no. 16, pp. R10653–R10656, 2000, doi: 10.1103/PhysRevB.62.R10653.

[7] I. Kang, M. J. Schulz, J. H. Kim, V. Shanov, and D. Shi, "A carbon nanotube strain sensor for structural health monitoring," *Smart Mater. Struct.*, vol. 15, no. 3, pp. 737–748, 2006, doi: 10.1088/0964-1726/15/3/009.

[8] R. Zhang, A. Dowden, H. Deng, M. Baxendale, and T. Peijs, "Conductive network formation in the melt of carbon nanotube/thermoplastic polyurethane composite," *Compos. Sci. Technol.*, vol. 69, no. 10, pp. 1499–1504, 2009, doi: 10.1016/j.compscitech.2008.11.039.

[9] R. Zhang et al., "Strain sensing behaviour of elastomeric composite films containing carbon nanotubes under cyclic loading," *Compos. Sci. Technol.*, vol. 74, pp. 1–5, 2013, doi: 10.1016/j.compscitech.2012.09.016.

[10] J. F. Christ, N. Aliheidari, A. Ameli, and P. Pötschke, "3D printed highly elastic strain sensors of multiwalled carbon nanotube/thermoplastic polyurethane nanocomposites," *Mater. Des.*, vol. 131, pp. 394–401, 2017, doi: 10.1016/j.matdes.2017.06.011.

[11] W. Huang et al., "Flexible and Lightweight Pressure Sensor Based on Carbon Nanotube/Thermoplastic Polyurethane-Aligned Conductive Foam with Superior Compressibility and Stability," *ACS Appl. Mater. Interfaces*, vol. 9, no. 48, pp. 42266–42277, 2017, doi: 10.1021/acsami.7b16975.

[12] J. F. Fennell et al., "Nanowire Chemical/Biological Sensors: Status and a Roadmap for the Future," *Angew. Chemie - Int. Ed.*, vol. 55, no. 4, pp. 1266–1281, 2016, doi: 10.1002/anie.201505308.

[13] V. Schroeder, S. Savagatrup, M. He, S. Lin, and T. M. Swager, "Carbon nanotube chemical sensors," *Chem. Rev.*, vol. 119, no. 1, pp. 599–663, 2019, doi: 10.1021/acs.chemrev.8b00340.

[14] J. T. W. Yeow and Y. Wang, "A review of carbon nanotubes-based gas sensors," *J. Sensors*, vol. 2009, 2009, doi: 10.1155/2009/493904.

[15] R. Tang, Y. Shi, Z. Hou, and L. Wei, "Carbon nanotube-based chemiresistive sensors," *Sensors*, vol. 17, no. 4, 2017, p. 882 doi: 10.3390/s17040882.

[16] T. Zhang, S. Mubeen, N. V. Myung, and M. A. Deshusses, "Recent progress in carbon nanotube-based gas sensors," *Nanotechnology*, vol. 19, no. 33, 2008, doi: 10.1088/0957-4484/19/33/332001.

[17] P. Biju, K. A. Jose, C. Anupama, and K. V. Vijay, "Carbon nanotube/PMMA composite thin films for gas-sensing applications," *Smart Mater. Struct.*, vol. 12, no. 6, 2003, pp. 935-939, doi: 10.1088/0964-1726/12/6/010

[18] C. Wei, L. Dai, A. Roy, and T. B. Tolle, "Multifunctional chemical vapor sensors of aligned carbon nanotube and polymer composites," *J. Am. Chem. Soc.*, vol. 128, no. 5, pp. 1412–1413, 2006, doi: 10.1021/ja0570335.

[19] S. Meer, A. Kausar, and T. Iqbal, "Trends in Conducting Polymer and Hybrids of Conducting Polymer/Carbon Nanotube: A Review," *Polym. - Plast. Technol. Eng.*, vol. 55, no. 13, pp. 1416–1440, 2016, doi: 10.1080/03602559.2016.1163601.

Recycling Opportunities for Lithium-ion Batteries. Review

Nataliya A. Gvozdik*

Abstract **The rate of Lithium-ion batteries (LIBs) production significantly exceeds the recycling capacities. Up to date, the final products of LIBs recycling are such primary raw materials as Li, Co and Ni. This process is ineffective and goes against the "circular economy" concept. However, other methods of recycling with re-use and refurbished basic materials of LIBs components have been developed. This review is aimed to cover the alternative methods of LIBs recycling without complete decomposition of the battery materials. We included a short overview of LIBs working principles, materials, and degradation mechanisms to illustrate working principles of alternative recycling approaches with the reintroduction of LIB compounds into the economy cycle.**

Index Terms **LIBs recycling, LIBs re-use, cathode regeneration, solid-boosters, anode recovering**

I. INTRODUCTION. LIFE CYCLE OF LIBS

As fuel-based transport produces one third of the CO_2 emissions, the world-wide direction to the decarbonization and the development of eco-friendly technologies has fostered the industry of electric vehicles [1]. Mass-production of the electrical cars implies a drastic increase in battery production as well [2]. The lithium-ion batteries are recognized as the most mature technology suitable for the electric transportation as they have a high energy density and reliability among with easy-to-install charge stations [3]. However, the life cycle of the LIBs is not adapted to the exponentially growing market. The demand in recycling of spent LIBs is expected to dramatically grow in next decade [4]. Hence, there is a tendency of government stimulation of recycling initiatives using legislative and financial resources [5].

The battery life has several steps. The battery stacks in electrical vehicles are recognized to be reliable and effective till the capacity reaches the minimum of 80% of initial ones, or another degradation phenomena arises [6]. Removed battery stacks are then used as stationary energy storage systems (ESS) for the next 10-15 years [7]. Such prolongation of battery utilization effectively shifts the recycling need to the future. However, LIBs re-use in ESS requires a standardization of form-factor, size, voltage output and other characteristics to make this transition widely spread. Rapid development of smart-grids is also needed [8]. Meanwhile, a huge amount of spent LIBs from portable electronics and stacks with irregular configurations will require recycling.

* Nataliya A. Gvozdik is with the Center of Energy Science and Technology, Skolkovo Institute of Science and Technology, Skolkovo Innovation Center, Building 3, Moscow 121205, Russia (e-mail: Natalyia.Gvozdik@skoltech.ru).

II. OPERATION PRINCIPLE OF LIBS

The four main components of a LIB are cathode, electrolyte, separator, and anode (Fig. 1). The anode stores lithium ions during charging, and the lithium ions move to the cathode during discharging to drive the electrical applications. Every electron pushed to the external circuit is compensated by the lithium ion which reacts ((de)intercalates) with cathode or anode material, causing the redox reaction in it. The degradation mechanisms attributed to these redox reactions are discussed below.

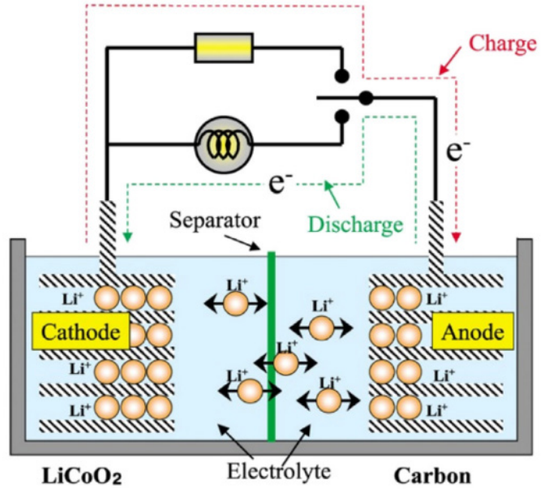

Fig. 1. Schematic principle of LIB. Reprinted with permission from [9].

III. DEGRADATION MECHANISMS IN LIBS

Widely used cathode materials include Lithium manganese oxide (LMO, $LiMn_2O_4$), Lithium iron phosphate (LFP, $LiFePO_4$), layered metal oxide like $Li[Ni_xCo_yMn_{1-x-y}]O_2$ (NCM) and Li-rich materials. Anode materials include graphite (C) and $Li_4Ti_5O_{12}$ (LTO). There are only several kinds of Li-ion cells with selected anode and cathode combinations including LFP/C, LMO/C, NCM/C, NCM/LTO, etc. LFP/C cells have a long life and high safety. Schematic illustration of possible degradation mechanisms is presented below (Fig. 2).

A. Anode degradation

The first degradation mechanism is observed at the anode. During the charging and discharging processes, there will be Li+ consumption coupled with the electrolyte decomposition, forming a passivation protective layer on the surface of graphite anode electrode, called SEI (solid electrolyte interface). The SEI film is mainly formed during the first few charging processes, especially during the first cycle, causing the fast degradation of the battery capacity.

Another problem relates to the anode volume fluctuation with the battery charging and discharging. The graphite material would have a volume change about 10% due to the lithium ions intercalation and deintercalation. The SEI film may crack, leading to the contact and reaction between the graphite and electrolyte resulting in extra irreversible lithium consumption. Excessive SEI thickness can block lithium ions pathways, reducing the available capacity. This continuous thickening of the SEI on the surface of graphite anode is widely accepted as one of the major reasons for LIBs aging [6].

Moreover, the lithium deposition due to the low temperature charging, fast charging or overcharging may lead to capacity decay, dendrites formation and shortening the cells. Copper corrosion and binder decomposition may result in loss of active material.

B. Cathode degradation

The LMO cathode material has the advantages of low price, high energy density and nontoxicity. Its main aging mechanisms are the structural deformation caused by Jahn-Teller distortion and dissolution of manganese. As a result, lithium ions accumulate on the surface of the LMO particles, and manganese changes its position in the crystal structure. One reason of it is tendency of Mn^{3+} to disproportionate into Mn^{2+} and Mn^{4+}. This disproportionation reaction happens at low potentials.

The LFP cathode has low voltage and low diffusion rate, resulting in low energy density. However, it has the long cycle life, low price, and safety. Currently, it is one of the most widely used LIBs cathode materials in commercial vehicles. Iron ions also dissolve slightly in the electrolyte. The iron ions may be reduced on the anode surface, catalyzing the SEI formation and resulting in increased internal resistance.

The NCM cathode has high energy density and low price. It has been widely used in passenger vehicles. The main aging mechanisms for NCM cathode may include: (i) crack formation due to the volume change during the charging and discharging cycle, (ii) dissolution of transition metal ions, (iii) generation of SEI film by side reaction between cathode materials and electrolyte [10].

Thus, practically all raw materials utilized in the LIBs do not degrade significantly in terms of their initial properties, but their assembly undergoes the chemical irreversible processes on the interfaces. The purification of surfaces coupled with lithium replenishment could be one of the possible ways to restore the battery capacity. However, proposed recycling processes are mainly aimed at mass utilization of LIBs with maximum economic efficiency and minimum CO_2 emissions [11].

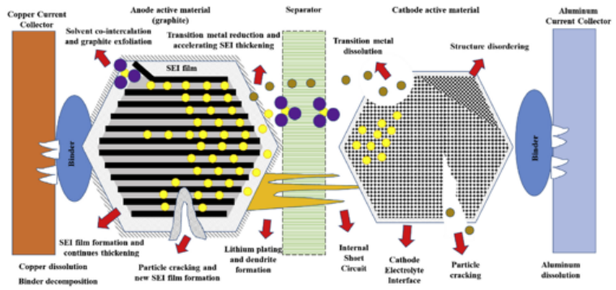

Fig. 2. Overview of main degradation mechanisms in LIBs. Reprinted with permission from [6].

IV. STANDARD PATHWAY OF LIBS RECYCLING

Currently, metallic components are recovered as alloys as a result of pyrometallurgical processes or, in the case of large casing materials, during mechanical dismantling. The remaining materials, such as Li compounds, electrolyte, plastics, and organic materials, are lost, except in China and South Korea, where Li is recovered as Li_2CO_3 [12].

In general, the following steps are performed to get the target compounds. Firstly, a battery disassembly under the CO_2 environment is followed by mechanical grinding. The precision of this step is significantly influenced by standardization requirements, robotics capabilities and targeting separation components [13].

Existing processes for recycling spent LIBs can be categorized into pyrometallurgy and hydrometallurgy. For the pyrometallurgical process, high energy consumption is required. Also toxic gases are formed during the burning. Pyrometallurgical metals reclamation uses a high-temperature furnace to reduce the component metal oxides to an alloy of Co, Cu, Fe and Ni. Hydrometallurgy is an advantageous process for the separation and complete recovery of metal ions with such benefits as low energy requirements and minimization of waste [14]. Hydrometallurgical treatments involve the use of aqueous solutions to leach the desired metals from cathode material. By far the most common combination of reagents reported is H_2SO_4/H_2O_2 mixture. Physical materials separation requires delicate separation components, thus, can be presented as another recycling method [13].

Even though LIBs are excellent secondary resources for lithium recovery, lithium recycling requires alternative methods for the whole process. The pyrometallurgy approach is ready to scale up; however, lithium is lost in the slag phase [15]. Hydrometallurgical methods result in poor recovery efficiency of lithium as it is reclaimed in the last step. This limits industrial Li recovery. However, proposed techniques in lab scale allowed effectively extracting of LiF [16]. To sum up, the existing recovery procedures implies complete decomposition of materials, which are the basic "know-how" of the whole technology. Meanwhile, alternative ways to recover the materials without loss of general structure are reviewed below.

V. ALTERNATIVE REUSE OF LIBS RESEARCH

Here we accumulated alternative methods of LIBs compounds recycling and reuse without complete decomposition.

A. Cathode material regeneration

Main degradation mechanisms of cathode materials are lithium depletion due to anode side reactions, transition metals dissolution and disordering. Generally, these problems can be addressed by heating of the material in presence of lithium source until intensive solid-state diffusion occurs [17].

For example, a method of resynthesis cathode NCM material was proposed based on facile co-extraction and co-precipitation processes [18]. Organic phase with metals was transformed into inorganic salt mixture by sulfuric acid, and the cathode material was directly regenerated from stripping liquor without separating metals individually by co-precipitation method. A more gentle way was demonstrated using eutectic Li^+ molten–salt solutions for ambient-pressure relithiation to recycle and remanufacture NCM cathode materials from 40% to 100% of lithium content (Fig. 3) [19].

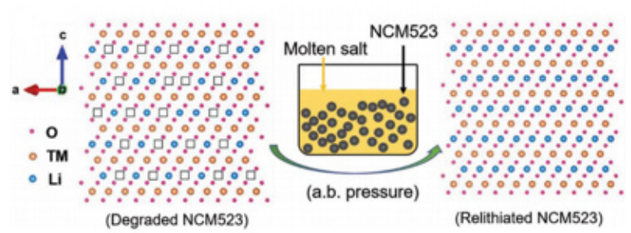

Fig. 3. Illustration of the relithiation process for Li composition recovery via the eutectic molten salt approach. Reprinted with permission from [19].

Electrochemical utilization of LFP was demonstrated at the lab scale for decomposition of this substance to the initial components, such as $FeSO_4$ and LiOH [20]. The main principle of the approach was a coincidence of redox potentials of soluble mediator and the cathode material, which dissolves during the electrochemical process. The final compounds had an extra purity. Another electrochemical method showed the effective extraction of $FeSO_4$ and Li_2CO_3 based on electrolysis in cell with anion-conductive membrane [21]. A more robust approach of LFP regeneration is to convert the graphitic anode to the conductive additive, followed by crystal structure regeneration under high temperatures [22].

B. Anode material regeneration

Industrial regeneration of graphite anodes has a lower added value than the above metal materials. However, lab scale methods were elaborated, where anode material was recycled from scrapped batteries with high yield through the recycling process. The first step was an effective removal of the residual conductive agent acetylene black, binder, thickener CMC and solid-electrolyte interphase from the recycled anode material by shearing emulsified in H_2SO_4/H_2O_2 solution, centrifugation and further heating in air at 300-600 °C for 1 hour [23]. Another method proposed a regeneration of graphite via pyrolyzation, acid leaching, graphitization and coating by amorphous carbon. As a result, material had negligible impurities, smaller specific surface area, reduced pore defects and higher degree of graphitization. Assembled LIBs exhibited a high initial coulombic efficiency of 90.64% and a high specific capacity of 344 mAh/g [24].

C. Alternative implementations of LIBs compounds

It was proposed to reuse the anode scrap of spent LIBs as high-performance cathode in Electro-Fenton systems with high efficiency [25]. Electro-Fenton process is an emerging treatment technology for wastewater. Electro-Fenton utilizes hydroxyl radicals to oxidize hazardous contaminants and is especially useful to treat persistent compounds that are not easily degraded in conventional water and wastewater treatment plants [26].

Another promising application of cathode materials in ESS is a flow battery with solid boosters [27], [28]. Particles of purifier cathode material can store extra energy. The organic molecules play a role of mediator and circulate in the system by transferring energy from the electrochemical cell to the reservoirs where the solid materials are stored.

There are several studies aiming to utilize cathode materials as catalysts for various reactions, like biomass pyrolysis or sulfate radical-based advance oxidation processes [29], [30]. Moreover, implementation of $LiCoO_2$ was also demonstrated as a promising electrocatalyst for the oxygen evolution reaction [31]. At the same time graphite anode material after pretreatment was recognized as effective additive to the catalysts for oxygen reduction reaction [32].

VI. CONCLUSIONS

Discussed methods of LIBs recycling provide an insight in the complexity of modern and future technological recycling challenges. Contemporary industrial approaches to LIBs recycling focus on the pure metal recovery, while alternative methods of compounds reuse and regeneration are gaining momentum. However, a lot of efforts and research is still needed to make these methods commercially viable. The complexity of recycling processes highlights the interrelations between many fields and industries.

VIII. REFERENCES

[1] J. Krause et al., "EU road vehicle energy consumption and CO2 emissions by 2050 – Expert-based scenarios," *Energy Policy*, vol. 138, no. January 2019, p. 111224, 2020.

[2] G. Harper et al., "Recycling lithium-ion batteries from electric vehicles," *Nature*, vol. 575, no. 7781, pp. 75–86, 2019.

[3] T. Fujita et al., "Reduction, reuse and recycle of spent Li-ion batteries for automobiles: A review," *Int. J. Miner. Metall. Mater.*, vol. 28, no. 2, pp. 179–192, 2021.

[4] W. Lv, Z. Wang, H. Cao, Y. Sun, Y. Zhang, and Z. Sun, "A Critical Review and Analysis on the Recycling of Spent Lithium-Ion Batteries," *ACS Sustain. Chem. Eng.*, vol. 6, no. 2, pp. 1504–1521, 2018.

[5] R. Deng, Y. Liu, W. Chen, and H. Liang, "A Survey on Electric Buses - Energy Storage, Power Management, and Charging Scheduling," *IEEE Transactions on Intelligent Transportation Systems*, vol. 22, no. 1, pp. 9–22, 2021.

[6] C. R. Birkl, M. R. Roberts, E. McTurk, P. G. Bruce, and D. A. Howey, "Degradation diagnostics for lithium ion cells," *J. Power Sources*, vol. 341, pp. 373–386, 2017.

[7] L. Ahmadi, S. B. Young, M. Fowler, R. A. Fraser, and M. A. Achachlouei, "A cascaded life cycle: reuse of electric vehicle lithium-ion battery packs in energy storage systems," *Int. J. Life Cycle Assess.*, vol. 22, no. 1, pp. 111–124, 2017.

[8] E. Martinez-Laserna et al., "Battery second life: Hype, hope or reality? A critical review of the state of the art," *Renew. Sustain. Energy Rev.*, vol. 93, no. April, pp. 701–718, 2018.

[9] Y. Nishi, "The development of lithium ion secondary batteries," *Chem. Rec.*, vol. 1, no. 5, pp. 406–413, 2001.

[10] X. Han et al., "A review on the key issues of the lithium ion battery degradation among the whole life cycle," *eTransportation*, vol. 1, p. 100005, 2019.

[11] R. E. Ciez and J. F. Whitacre, "Examining different recycling processes for lithium-ion batteries," *Nat. Sustain.*, vol. 2, no. 2, pp. 148–156, 2019.

[12] O. Velázquez-Martínez, J. Valio, A. Santasalo-Aarnio, M. Reuter, and R. Serna-Guerrero, "A critical review of lithium-ion battery recycling processes from a circular economy perspective," *Batteries*, vol. 5, no. 4, pp. 5–7, 2019.

[13] E. Fan et al., "Sustainable Recycling Technology for Li-Ion Batteries and Beyond: Challenges and Future Prospects," *Chem. Rev.*, vol. 120, no. 14, pp. 7020–7063, 2020.

[14] S. Natarajan, A. B. Boricha, and H. C. Bajaj, "Recovery of value-added products from cathode and anode material of spent lithium-ion batteries," *Waste Manag.*, vol. 77, pp. 455–465, 2018.

[15] C. Liu, J. Lin, H. Cao, Y. Zhang, and Z. Sun, "Recycling of spent lithium-ion batteries in view of lithium recovery: A critical review," *J. Clean. Prod.*, vol. 228, no. 1, pp. 801–813, 2019.

[16] Y. Zheng, W. Song, W. T. Mo, L. Zhou, and J. W. Liu, "Lithium fluoride recovery from cathode material of spent lithium-ion battery," *RSC Adv.*, vol. 8, no. 16, pp. 8990–8998, 2018.

[17] Y. Zhao et al., "Regeneration and reutilization of cathode materials from spent lithium-ion batteries," *Chem. Eng. J.*, vol. 383, p. 123089, 2020.

[18] Y. Yang, S. Xu, and Y. He, "Lithium recycling and cathode material regeneration from acid leach liquor of spent lithium-ion battery via facile co-extraction and co-precipitation processes," *Waste Manag.*, vol. 64, pp. 219–227, 2017.

[19] Y. Shi, M. Zhang, Y. S. Meng, and Z. Chen, "Ambient-Pressure Relithiation of Degraded $Li_xNi_{0.5}Co_{0.2}Mn_{0.3}O_2$ (0< x< 1) via Eutectic Solutions for Direct Regeneration of Lithium-Ion Battery Cathodes," *Adv. Energy Mater.*, vol. 9, no. 20, p. 1900454, 2019.

[20] J. Yu, X. Wang, M. Zhou, and Q. Wang, "A redox targeting-based material recycling strategy for spent lithium ion batteries," *Energy Environ. Sci.*, vol. 12, no. 9, pp. 2672–2677, 2019.

[21] Z. Li, D. F. Liu, J. Xiong, L. He, Z. Zhao, and D. Wang, "Selective recovery of lithium and iron phosphate/carbon from spent lithium iron phosphate cathode material by anionic membrane slurry electrolysis," *Waste Manag.*, vol. 107, pp. 1–8, 2020.

[22] W. Song et al., "Re-synthesis of nano-structured $LiFePO_4$/graphene composite derived from spent lithium-ion battery for booming electric vehicle application," *J. Power Sources*, vol. 419, pp. 192–202, 2019.

[23] J. Zhang, X. Li, D. Song, Y. Miao, J. Song, and L. Zhang, "Effective regeneration of anode material recycled from scrapped Li-ion batteries," *J. Power Sources*, vol. 390, pp. 38–44, 2018.

[24] D. Ruan et al., "A high-performance regenerated graphite extracted from discarded lithium-ion batteries," *New J. Chem.*, vol. 45, no. 3, pp. 1535–1540, 2021.

[25] Z. Cao et al., "Efficient reuse of anode scrap from lithium-ion batteries as cathode for pollutant degradation in electro-Fenton process: Role of different recovery processes," *Chem. Eng. J.*, vol. 337, pp. 256–264, 2018.

[26] H. He and Z. Zhou, "Electro-fenton process for water and wastewater treatment," *Crit. Rev. Environ. Sci. Technol.*, vol. 47, no. 21, pp. 2100–2131, 2017.

[27] J. F. Vivo-Vilches, A. Nadeina, N. Rahbani, V. Seznec, D. Larcher, and E. Baudrin, "$LiFePO_4$-ferri/ferrocyanide redox targeting aqueous posolyte: Set-up, efficiency and kinetics," *J. Power Sources*, vol. 488, p. 229387, 2021.

[28] S. Gentil, D. Reynard, and H. H. Girault, "Aqueous organic and redox-mediated redox flow batteries: a review," *Current Opinion in Electrochemistry*, vol. 21, pp. 7–13, 2020.

[29] L. Chen, P. Wang, Y. Shen, and M. Guo, "Spent lithium-ion battery materials recycling for catalytic pyrolysis or gasification of biomass," *Bioresour. Technol.*, vol. 323, p. 124584, 2021.

[30] X. Wang et al., "Recycling the Cathode Scrap of Spent Lithium-Ion Batteries as an Easily Recoverable Peroxymonosulfate Catalyst with Enhanced Catalytic Performance," *ACS Sustain. Chem. Eng.*, vol. 8, no. 30, pp. 11337–11347, 2020.

[31] V. C. B. Pegoretti, P. V. M. Dixini, L. Magnago, A. K. S. Rocha, M. F. F. Lelis, and M. B. J. G. Freitas, "High-temperature (HT) $LiCoO_2$ recycled from spent lithium ion batteries as catalyst for oxygen evolution reaction," *Mater. Res. Bull.*, vol. 110, pp. 97–101, 2019.

[32] D. Ruan et al., "Recycling of Graphite Anode from Spent Lithium-ion Batteries for Preparing Fe-N-doped Carbon ORR Catalyst," *ChemCatChem*, p. cctc.202001867, 2021.